Progress In Electromagnetics Research Letters, Vol. 101, 63–70, 2021

Design of Full-360° Reflection-Type Phase Shifter Using Trans-Directional Coupler with Multi-Resonance Loads

Hongmei Liu*, Xuejiao Wang, Tielin Zhang, Shaojun Fang, and Zhongbao Wang

Abstract—In this paper, a full-360° reflection-type phase shifter (RTPS) using a trans-directional (TRD) coupler with multi-resonance loads is presented. It features the characteristics of wide bandwidth, small size, wide phase shifts with a compact structure and inherent DC blocking. Influences of the multi-resonance loads on the phase shifts and insertion losses of the RTPS are analyzed, and design procedures are given for guidance. For validation, a prototype is designed at 2 GHz. The overall size is $0.56\lambda_g \times 0.17\lambda_g$. Measured results show a bandwidth of 20% under the criterion of more than 10-dB return loss. Meanwhile, a relative phase variation of 425° with a maximum insertion loss of 3.6 dB is achieved when the varactor capacitance is varied among 0.35 pF $\sim$ 3.2 pF.

1. INTRODUCTION

As an indispensable component in modern wireless communication systems, phase shifters are widely used in phased-array antenna systems [1, 2], phase-modulation communication systems [3], and harmonic distortion cancellation [4]. Among the analog phase shifters, reflection type phase shifter (RTPS), which consists of a 3-dB quadrature coupler with two identical tunable reflection loads, provides a balanced compromise among phase variation range, insertion loss, and compactness compared with loaded transmission line [5] and switched network [6] phase shifters.

In the design of RTPS, a tradeoff among phase variation, bandwidth, and compactness should be considered. However, the conventional structure exhibits a restricted phase shift over a narrow band. Since the superiority of a phase shifter is generally determined by the maximum phase variation range, several approaches have been proposed for this issue. In [7], a low loss RTPS with a relative phase variation of 190° is achieved by using a stub loaded quadrature coupler with reduced varactors. By using an impedance transforming quadrature coupler with equalized series-resonated varactors, a phase shift tuning range of 237° is obtained [8]. Further, a maximal relative phase shift of 407° is realized by replacing the series-resonated varactors [8] with cascaded connections of varactors [9]. A π-type network consisting of three varactors is reported to achieve a phase shift of 385° [10]. In [11], an RTPS composed of two transformer-based quadrature couplers and two transformer-based multi-resonance loads provides a phase shift of 367°. However, since branch lines are used for constructing the coupler, all these reports can only exhibit a bandwidth around 10%. Besides, large size is also the disadvantage. Although a packaged chip coupler is used in [12] for size reduction, the overall size is still large, and the bandwidth is limited (about 10%).

To address the problem of narrow bandwidth, short-ended coupled lines are proposed, and a bandwidth of 36% is achieved [13]. However, the maximum phase variation is limited to 255°. In addition, slotted ground plane with shunt capacitor has to be used for realizing a high value of even-mode impedance and tight coupling. Further bandwidth enhancement (66.7%) can be obtained by using a vertically installed planar (VIP) coupled-line coupler [14]. A phase variation of 350° is realized at the

Received 18 September 2021, Accepted 24 November 2021, Scheduled 6 December 2021
* Corresponding author: Hongmei Liu (lhm323@dlmu.edu.cn).
The authors are with the School of Information Science and Technology, Dalian Maritime University, Dalian, Liaoning 116026, China.

center frequency. For single-layer PCB implementation, a coupled line based tight-coupling coupler is applied in [15]. The maximum phase shift of 392° is obtained by using the reflection loads in [10].

Except branch line (BL) and coupled line (CL) couplers, there also exists another type of directional couplers, named as coupled line trans-directional (CL-TRD) coupler. It shows wider bandwidth and smaller size than a BL coupler. Moreover, tight coupling and easy connection with external circuits [16] are the advantages compared with a CL coupler. Besides, between the input and output ports of a CL-TRD coupler, DC blocking is inherent. Recently, several researches have been done on the TRD-based RTPS [17–19]. However, the phase shift ranges of these reports are limited to less than 180°.

In the paper, the CL-TRD coupler previously proposed in [19], which has a balanced output ports power distribution and phase performance, is applied to the construction of an RTPS. To achieve full 360° phase shift, multi-resonance loads are connected. The measurement results show that the proposed RTPS exhibits an excellent tradeoff among phase variation, bandwidth, and compactness.

2. THEORETICAL ANALYSIS

Figure 1 shows the schematic of the proposed RTPS, which consists of a 3-dB CL-TRD coupler [20] loaded by two identical reflection loads. Each reflection load is composed of two inductors named L_1 and L_2 and two identical varactor diodes named D_1. One varactor is connected in parallel to inductor L_1, forming a parallel-resonated circuit. The addition of inductor L_2 in series with the varactor will increase the equivalent capacitance of the varactor, which results in wide phase shift. Moreover, an additional varactor is paralleled for extending the phase shift range without causing extra insertion loss.

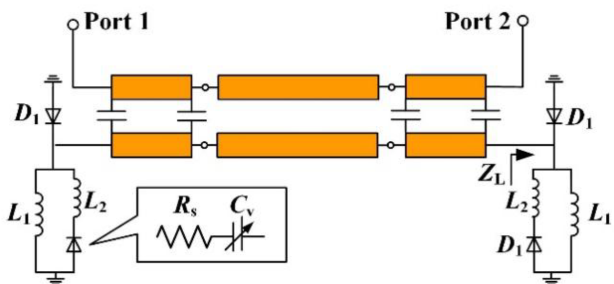

Figure 1. Schematic of the proposed RTPS.

In the analysis, varactor diode D_1 is modeled as a parasitic resistor R_s in series with the tunable capacitor C_v for simplifying the calculation, as shown in Fig. 1. Thus, the load impedance Z_L can be expressed as

$$Z_L = \frac{T_1 + \mathrm{j}T_2}{T_3/Z_0 + \mathrm{j}T_4/Z_0} \tag{1}$$

Then, the reflection coefficient can be obtained as

$$\begin{aligned}\Gamma &= \frac{Z_L - Z_0}{Z_L + Z_0} \\ &= \frac{\sqrt{\left[(T_1 - T_3)(T_1 + T_3) + (T_2 - T_4)(T_2 + T_4)\right]^2 + \left[(T_1 + T_3)(T_2 - T_4) - (T_1 - T_3)(T_2 + T_4)\right]^2}}{(T_1 + T_3)^2 + (T_2 + T_4)^2} \\ &\quad e^{\mathrm{j}\arctan\frac{(T_1+T_3)(T_2-T_4)-(T_1-T_3)(T_2+T_4)}{(T_1-T_3)(T_1+T_3)+(T_2-T_4)(T_2+T_4)}}\end{aligned} \tag{2}$$

where

$$T_1 = -\omega^4 L_1 L_2 R_S C_v^2 + 2\omega^2 L_1 R_S C_v \tag{3a}$$

$$T_2 = \omega^3 L_1 R_S^2 C_v^2 + \omega^3 L_1 L_2 C_v - \omega L_1 \tag{3b}$$

$$T_3 = Z_0 \left[\omega^2 C_v (2L_1 + L_2) + \omega^2 C_v^2 R_S^2 - \omega^4 L_1 L_2 C_v^2 - 1\right] \tag{3c}$$

$$T_4 = Z_0 \left[\omega^3 R_S C_v^2 (2L_1 + L_2) - 2\omega C_v R_S\right] \tag{3d}$$

Here, Z_0 is equal to $50\,\Omega$. According to Eq. (2), the maximum shift $\Delta\varphi$ and the insertion loss (IL) are obtained, as listed in Eq. (4).

$$\Delta\varphi = |\varphi_{\max} - \varphi_{\min}| \tag{4a}$$

$$\mathrm{IL} = |\Gamma|^2 = \frac{\left[(T_1 - T_3)(T_1 + T_3) + (T_2 - T_4)(T_2 + T_4)\right]^2 + \left[(T_1 + T_3)(T_2 - T_4) - (T_1 - T_3)(T_2 + T_4)\right]^2}{\left[(T_1 + T_3)^2 + (T_2 + T_4)^2\right]^2} \tag{4b}$$

In Eq. (4a), $\varphi_{\max}$ and $\varphi_{\min}$ are the phase shifts at the maximum and minimum capacitance value, respectively. It can be found that $\Delta\varphi$ and IL are mainly affected by the capacitance C_v.

In order to express the variations more clearly, the curves of $\Delta\varphi$ and IL versus C_v and L_1 with different values of L_2 are plotted, as shown in Figs. 2 and 3. Here, the values of L_1 and C_v are gradually increased in the range of $3\,\mathrm{nH} \sim 20\,\mathrm{nH}$ and $0 \sim 10\,\mathrm{pF}$, respectively. While the value of L_2 starts from $2\,\mathrm{nH}$ to $14\,\mathrm{nH}$ with an interval of $4\,\mathrm{nH}$. It is observed from the four groups of curves that the ILs are decreased when the value of L_2 is increased. While the IL is slightly increased along with the increase of L_1. However, the values of L_2 cannot be infinitely large due to practical considerations. Besides, the phase shift will be damaged with large inductances. It is seen from Fig. 2 that the phase shift becomes more steep with the increase of L_2. Besides, smaller values of C_v are needed for full 360° phase shift. For example, when the value of L_2 is equal to $14\,\mathrm{nH}$, a full 360° phase shift can be realized with C_v in the range of $0.1\,\mathrm{pF} \sim 1.3\,\mathrm{pF}$. Nearly no phase shifting is observed for C_v larger than $2\,\mathrm{pF}$. However, the selection of varactors with capacitance variations of $0.1\,\mathrm{pF} \sim 1.3\,\mathrm{pF}$ is difficult. Thus, the range of L_2 is selected within $6\,\mathrm{nH} \sim 10\,\mathrm{nH}$.

When the value of L_2 is fixed, the selection of L_1 should be in consideration of the IL. It is observed from Fig. 3 that the IL is increased with the decrease of L_1. In detail, when L_2 is in the range of $6\,\mathrm{nH} \sim 10\,\mathrm{nH}$, the IL of less than $3.5\,\mathrm{dB}$ can be obtained for L_1 greater than $6\,\mathrm{nH}$. Besides the IL, the value of L_1 also affects the phase shift range although slightly. It is found from Fig. 2 that the phase shift range is decreased by 40° when L_1 increases from $6\,\mathrm{nH}$ to $20\,\mathrm{nH}$, while the IL is changed within $0.4\,\mathrm{dB}$. Thus, a smaller value of L_1 is preferred for obtaining large phase shift. In consideration of the

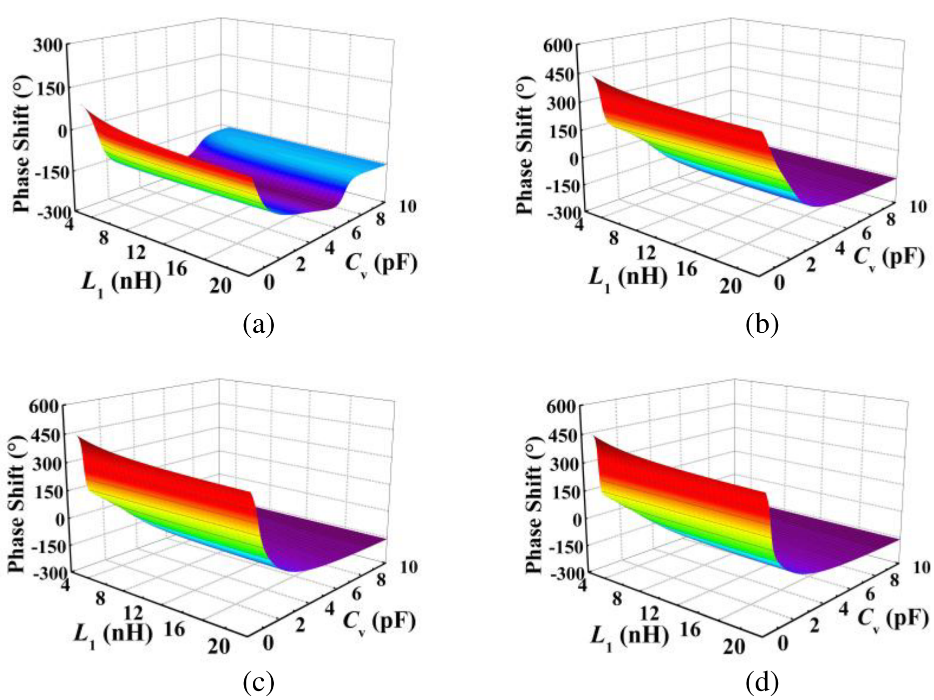

Figure 2. The curves of $\Delta\varphi$ versus C_v and L_1 ($f = 2\,\mathrm{GHz}$). (a) $L_2 = 2\,\mathrm{nH}$. (b) $L_2 = 6\,\mathrm{nH}$. (c) $L_2 = 10\,\mathrm{nH}$. (d) $L_2 = 14\,\mathrm{nH}$.

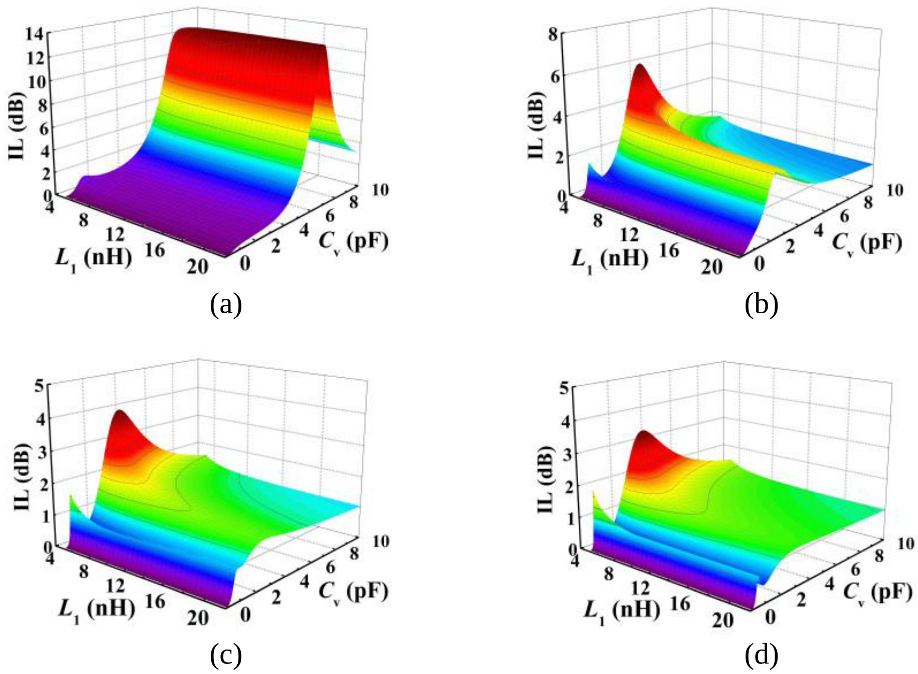

Figure 3. The curves of IL versus C_v and L_1 ($f = 2\,\text{GHz}$). (a) $L_2 = 2\,\text{nH}$. (b) $L_2 = 6\,\text{nH}$. (c) $L_2 = 10\,\text{nH}$. (d) $L_2 = 14\,\text{nH}$.

analysis investigated above, the design procedures are given for the proposed RTPS.

1. Using Eqs. (4a) and (4b), the variation trends of maximum shift $\Delta\varphi$ and IL can be plotted with different values of L_1, L_2, and varactor capacitance.
2. According to the design requirements including the phase shifts and IL, determine the values of L_1, L_2, and varactor capacitance range.
3. According to the varactor capacitance range, choose suitable varactor.

3. IMPLEMENTATION AND RESULTS

For validation, a prototype operating at 2 GHz is designed and fabricated on an F4B substrate with a dielectric constant of 3.5, loss tangent of 0.003, and thickness of 1.5 mm. Fig. 4 shows the layout and photograph of the fabricated prototype. The overall size of the circuit is $50.7\,\text{mm} \times 15.2\,\text{mm}$

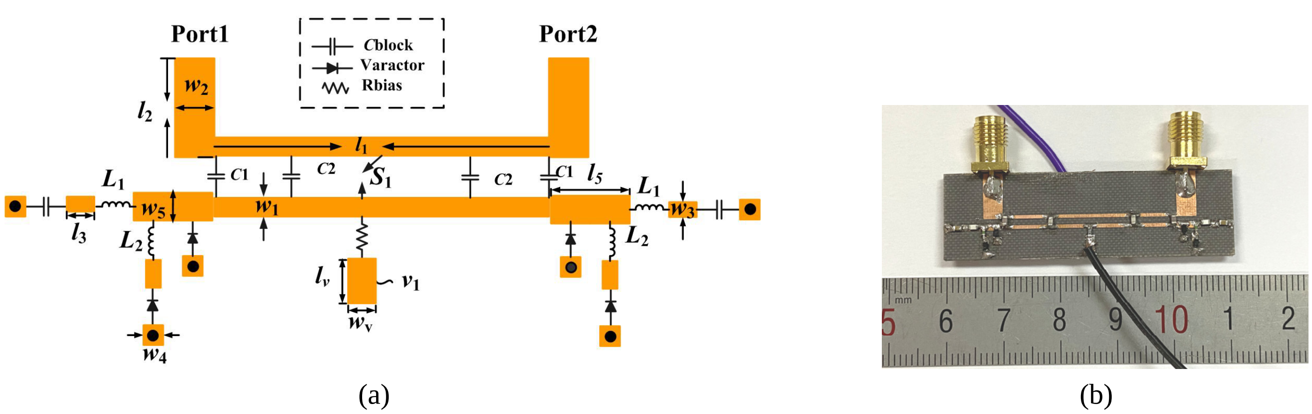

Figure 4. (a) Layout and (b) photograph of the proposed RTPS.

Table 1. Final dimensions of the prototype (unit: mm).

w_1	w_2	w_3	w_4	w_5	w_v
0.6	3.38	1	1	1	1.5
l_1	l_2	l_3	l_5	l_v	s_1
30.4	8	1.5	2	3	1.1
C_1	C_2	L_1	L_2	R_1	
0.7 pF	1.2 pF	8.2 nH	7.5 nH	10 kΩ	

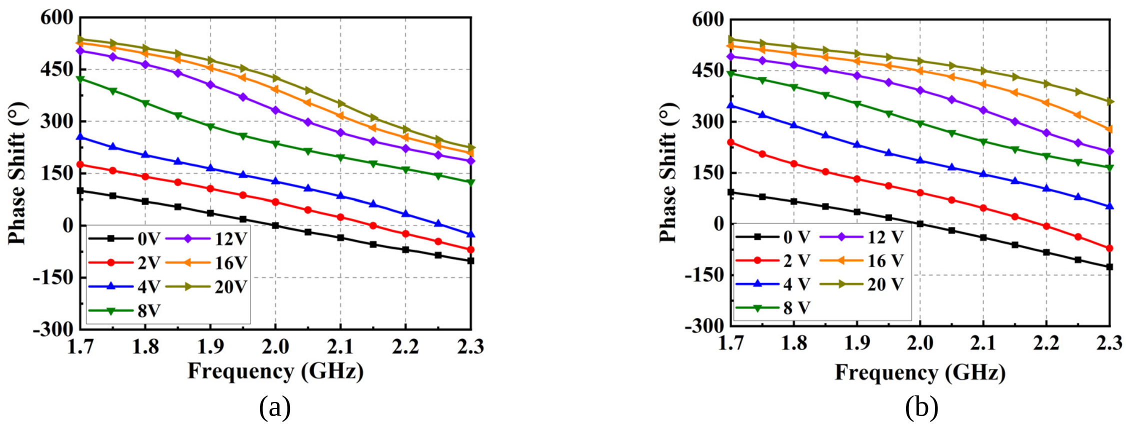

Figure 5. (a) Measured and (b) simulated phase shift of the prototype.

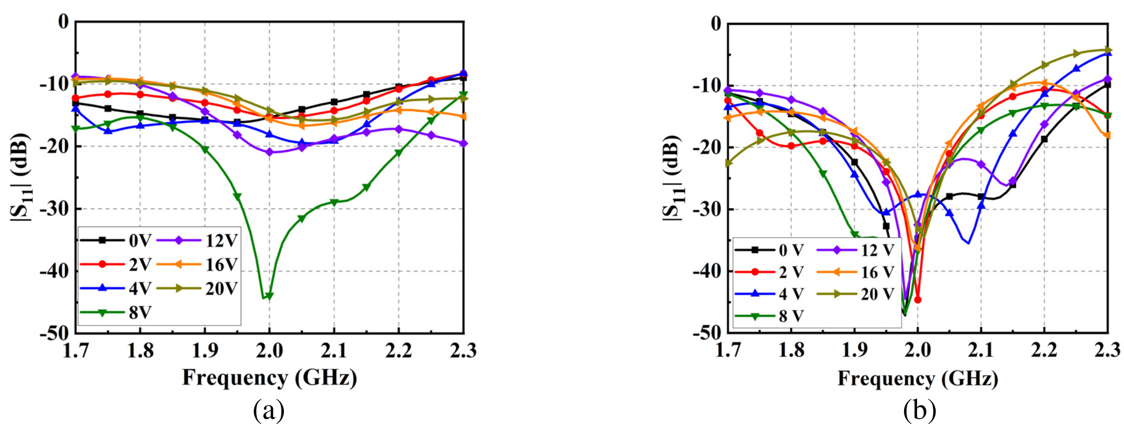

Figure 6. (a) Measured and (b) simulated $|S_{11}|$ of the prototype.

$(0.56\lambda_g \times 0.17\lambda_g)$. Table 1 illustrates the optimized final dimensions of the prototype. After optimizing by ADS, the final values of L_1 and L_2 are selected as 8.2 nH and 7.5 nH, respectively. The varactor is replaced by SMV2020-079LF ($C_{\min} = 0.35\,\text{pF}$, $C_{\max} = 3.2\,\text{pF}$) with the parasitic resistance R_s of $2.5\,\Omega$ and bias voltage range of $0 \sim 20\,\text{V}$. The capacitors C_1 and C_2 are replaced by commercial Murata GRM1855 series, while the inductors L_1 and L_2 are replaced by Murata LQG15 series.

The fabricated prototype is measured using Agilent N5230A. Figs. 5–7 show the simulated and measured results in the frequency range of $1.7\,\text{GHz} \sim 2.3\,\text{GHz}$. It is observed that when the reverse voltage is tuned from 0 V to 20 V, the total phase shift of 478° is achieved in simulation, while a measurement phase shift of 425° is obtained. During the tuning, the simulated and measured bandwidths

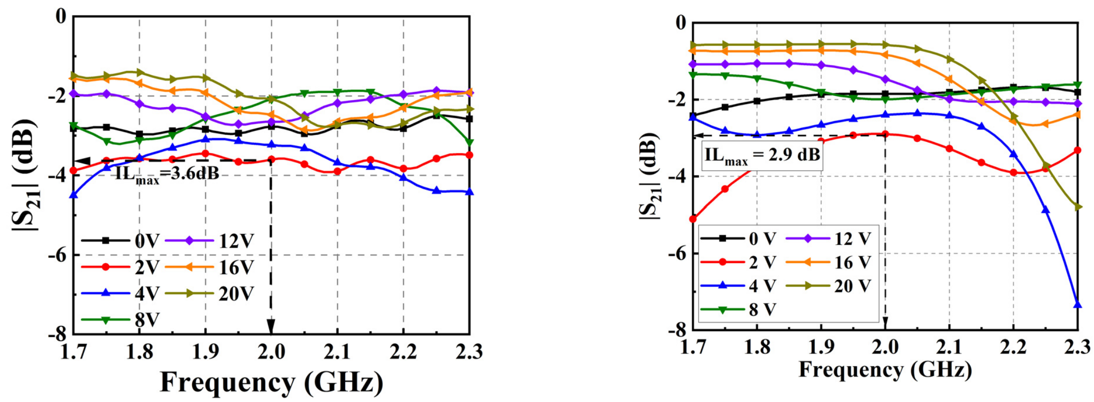

(a) (b)

Figure 7. (a) Measured and (b) simulated $|S_{21}|$ of the prototype.

for $|S_{11}| < -10$ dB are 1.83 GHz $\sim$ 2.23 GHz (20%) and 1.71 GHz $\sim$ 2.14 GHz (21.5%), respectively. At the center frequency, the measured $|S_{11}|$ are all less than -14 dB, while the simulated value is -15 dB. From Fig. 7, it is seen that at the center frequency, the simulated and measured maximum ILs are 2.9 dB and 3.6 dB, respectively. In the operation band, the values are less than 4.3 dB and 4.95 dB.

Table 2 shows the comparisons among the proposed and reported RTPSs. Compared with the branch-line (BL) coupler based RTPSs in [9] and [10], the proposed RTPS exhibits doubled bandwidth, smaller size, and wider phase shifts. Although the packaged chip is used in [12] for realizing the 3-dB coupler, the overall size is still large. Besides, the bandwidth and IL are needed to be improved. In comparison with the coupled-line (CL) coupler based RTPSs in [14] and [15], smaller size and wider phase shifts are also the advantages of the designed work. In [14], a VIP structure has to be applied for tight coupling. Besides, since the input/output ports of the proposed RTPS are on the same side, one power supply is enough. While two power supplies are needed for the CL coupler based RTPS. The proposed RTPS also inherits the DC blocking characteristic of the TRD coupler, with no need for the DC block capacitors. In summary, the proposed full-360° RTPS shows wide bandwidth, small size, wide phase shifts with a compact structure and inherent DC blocking, which can be a good candidate for modern wireless communication applications.

Table 2. Comparisons among the proposed and reported RTPSs.

Ref.	[9]	[10]	[12]	[14]	[15]	[19]	**This work**
Freq. (GHz)	2	2	5.85	1.5	10	2.15	**2**
IL[a] (dB)	4.6	1.56	> 4.3	2.6	3.4	0.72	**3.6**
RL[a] (dB)	19	13.4	16	15	> 10	19	**14**
Max. $\Delta\varphi^a$ (°)	407	385	360	350	392	121	**425**
FBW (%)	10	11	10.3	66.7	20	32	**20**
FoM[c] (°/dB)	88	246	< 84	135	115	169	**118**
Size[d] (λ_g^2)	0.19	0.11	0.09	0.10	0.25	0.03	**0.05**
Coupler type	BL	BL	Packaged chip	CL	CL	TRD	**TRD**

[a] Values at the center frequency. [b] $|S_{11}| < -10$ dB.

[c] FoM $= \Delta\varphi/|S_{21}|_{\max}$. [d] Dimensions without the input/output 50 Ω transmission lines.

4. CONCLUSION

In this paper, a full-360° reflection-type phase shifter (RTPS) with the features of wide bandwidth, small size, wide phase shifts, compact structure, and inherent DC blocking is presented. By using the CL-TRD coupler, the difficulty in physical realization can be reduced without narrow coupling gap nor non-planar circuit structure. Wide phase shifts are obtained with multi-resonance loads. For validation, a prototype operating at 2 GHz is designed. The measurement results and comparisons indicate that the proposed RTPS can be a good candidate for modern wireless communication applications.

ACKNOWLEDGMENT

This work was supported in part by the National Natural Science Foundation of China under Grant 51809030 and Grant 61871417, in part by the Natural Science Foundation of Liaoning Province under Grant 2020-MS-127, in part by the Liaoning Revitalization Talents Program under Grant XLYC2007067, in part by the Dalian Youth Science and Technology Star Project under Grant 2020RQ007 and in part by the Fundamental Research Funds for the Central Universities under Grant 3132021231.

REFERENCES

1. Yang, B., X. Chen, J. Chu, T. Mitani, and N. Shinohara, "A 5.8-GHz phased array system using power-variable phase-controlled magnetrons for wireless power transfer," *IEEE Trans. Microw. Theory Tech.*, Vol. 68, No. 11, 4951–4959, Nov. 2020.
2. Ren, H., P. Li, Y. Gu, and B. Arigong, "Phase shifter-relaxed and control-relaxed continuous steering multiple beamforming 4 × 4 butler matrix phased array," *IEEE Trans. Circuits Syst. I, Reg. Papers*, Vol. 67, No. 12, 5031–5039, Dec. 2020.
3. Yang, X. and J. Lin, "A digitally controlled constant envelope phase-shift modulator for low-power broad-band wireless applications," *IEEE Trans. Microw. Theory Techn.*, Vol. 54, No. 1, 96–105, Jan. 2006.
4. Sobhy, E. A. and S. Hoyos, "A multiphase multipath technique with digital phase shifters for harmonic distortion cancellation," *IEEE Trans. Circuits Syst. II, Exp. Briefs*, Vol. 57, No. 12, 921–925, Dec. 2010.
5. Bourtoutian, R. and P. Ferrari, "Tapered distributed analogue tunable phase shifter with low insertion and return loss," *IET Electron. Lett.*, Vol. 41, No. 15, 852–854, Jul. 2005.
6. Anand, P., S. Sharma, D. Sood, and C. C. Tripathi, "Design of compact reconfigurable switched line microstrip phase shifters for phased array antenna," *Proc. Emerg. Technol. Trends Electron. Commun. Netw.*, Vol. 19, 1–3, Gujarat, India, Dec. 2012.
7. Singh, A. and M. K. Mandal, "Electronically tunable reflection type phase shifters," *IEEE Trans. Circuits Syst. II, Exp. Briefs*, Vol. 67, No. 3, 425–429, Mar. 2020.
8. Lin, C., S. Chang, C. Chang, and Y. Shu, "Design of a reflection-type phase shifter with wide relative phase shift and constant insertion loss," *IEEE Trans. Microw. Theory Tech.*, Vol. 55, No. 9, 1862–1868, Sept. 2007.
9. Lin, C., S. Chang, and W. Hsiao, "A full-360° reflection-type phase shifter with constant insertion loss," *IEEE Microw. Wireless Compon. Lett.*, Vol. 18, No. 2, 106–108, Feb. 2008.
10. Burdin, F., Z. Iskandar, F. Podevin, and P. Ferrari, "Design of compact reflection-type phase shifters with high figure-of-merit," *IEEE Trans. Microw. Theory Tech.*, Vol. 63, No. 6, 1883–1893, Jun. 2015.
11. Li, T. and H. Wang, "A millimeter-wave fully integrated passive reflection-type phase shifter with transformer-based multi-resonance loads for 360° phase shifting," *IEEE Trans. Circuits Syst. I, Reg. Papers*, Vol. 65, No. 4, 1406–1419, Apr. 2018.
12. Vilenskiy, A. R., M. N. Makurin, E. I. Poshisholina, and C. Lee, "Design technique for varactor analog phase shifters with equalized losses," *Progress In Electromagnetics Research C*, Vol. 86, 1–16, 2018.

13. Abbosh, A. M., "Compact tunable reflection phase shifters using short section of coupled lines," *IEEE Trans. Microw. Theory Tech.*, Vol. 60, No. 8, 2465–2472, Aug. 2012.
14. Liu, W. J., S. Y. Zheng, Y. M. Pan, Y. X. Li, and Y. L. Long, "A wideband tunable reflection-type phase shifter with wide relative phase shift," *IEEE Trans. Circuits Syst. II, Exp. Briefs*, Vol. 64, No. 12, 1442–1446, Dec. 2017.
15. Venter, J. J. P., T. Stander, and P. Ferrari, "X-band reflection-type phase shifters using coupled-line couplers on single-layer RF PCB," *IEEE Microw. Wireless Compon. Lett.*, Vol. 28, No. 9, 807–809, Sept. 2018.
16. Shie, C. I., J. C. Cheng, S. C. Chou, et al., "Trans-directional coupled-line couplers implemented by periodical shunt capacitors," *IEEE Trans. Microw. Theory Tech.*, Vol. 57, No. 12, 2981–2987, Dec. 2009.
17. Sychev, A. N., I. M. Dobush, N. Y. Rudyi, and S. M. Struchkov, "Analog phase shifter of X-band implemented with novel trans-directional coupled-line coupler," *Proc. 48th Eur. Microw. Conf. (EuMC)*, 811–814, 2018.
18. Sychev, A. N., N. Y. Rudyi, I. M. Dobush, and K. K. Zharov, "A phase shifter based on trans-directional coupler with DC isolation of RF-path and control circuit," *Proc. APEIE*, 380–383, Novosibirsk, Russia, Oct. 2018.
19. Occello, O., L. Tiague, M. Margalef-Rovira, L. Vincent, F. Ndagijimana, and P. Ferrari, "High-performance compact reflection-type phase shifter operating at 2 GHz using a transdirectional coupler," *Proc. 50th Eur. Microw. Conf. (EuMC)*, 550–553, 2021.
20. Liu, H., S. Fang, Z. Wang, and T. Shao, "Coupled line trans-directional coupler with improved power distribution and phase performance," *Proc. IEEE Int. Symp. Radio-Frequency Integr. Technol. (RFIT)*, 126–128, Aug. 2017.